

Thermal Hall conductivity in the cuprate Mott insulators Nd_2CuO_4 and $\text{Sr}_2\text{CuO}_2\text{Cl}_2$

Marie-Eve Boulanger¹, Gaël Grissonnanche¹, Sven Badoux¹, Andréanne Allaire¹, Étienne Lefrançois¹, Anaëlle Legros^{1,2}, Adrien Gourgout¹, Maxime Dion¹, C. H. Wang³, X. H. Chen³, R. Liang⁴, W. N. Hardy⁴, D. A Bonn⁴ and Louis Taillefer^{1,5}

1 Institut Quantique, Département de physique & RQMP, Université de Sherbrooke, Sherbrooke, Québec J1K 2R1, Canada

2 SPEC, CEA, CNRS-UMR3680, Université Paris-Saclay, Gif-sur-Yvette, France

3 Hefei National Laboratory for physical Science at Microscale and Department of Physics, University of Science and Technology of China, Hefei, Anhui 230026, People's Republic of China

4 Department of Physics & Astronomy, University of British Columbia, Vancouver, British Columbia V6T 1Z1, Canada

5 Canadian Institute for Advanced Research, Toronto, Ontario M5G 1M1, Canada

The heat carriers responsible for the unexpectedly large thermal Hall conductivity of the cuprate Mott insulator La_2CuO_4 were recently shown to be phonons. However, the mechanism by which phonons in cuprates acquire chirality in a magnetic field is still unknown. Here, we report a similar thermal Hall conductivity in two cuprate Mott insulators with significantly different crystal structures and magnetic orders – Nd_2CuO_4 and $\text{Sr}_2\text{CuO}_2\text{Cl}_2$ – and show that two potential mechanisms can be excluded – the scattering of phonons by rare-earth impurities and by structural domains. Our comparative study further reveals that orthorhombicity, apical oxygens, the tilting of oxygen octahedra and the canting of spins out of the CuO_2 planes are not essential to the mechanism of chirality. Our findings point to a chiral mechanism coming from a coupling of acoustic phonons to the intrinsic excitations of the CuO_2 planes.

In the last decade, the thermal Hall effect has emerged as a new probe of insulators¹, materials in which the electrical Hall effect is zero because there are no mobile charged carriers. In the presence of a heat current \mathbf{J} along the x axis and a magnetic field \mathbf{H} along the z axis, a transverse temperature gradient ∇T (along the y axis) – and the associated thermal Hall conductivity κ_{xy} – can develop even if the carriers of heat are neutral (chargeless), provided they have chirality. (Here we use the term chirality to mean handedness in the presence of a magnetic field.) It has been shown that in certain conditions spins can produce such chirality². For example, magnons give rise to a thermal Hall signal in the antiferromagnet $\text{Lu}_2\text{V}_2\text{O}_7$ (ref. 3). As a result, a measurement of the thermal Hall effect can in principle provide access to various topological excitations in insulating quantum materials, such as Majorana edge modes in chiral spin liquids⁴. Recently, the thermal Hall conductivity κ_{xy} seen in $\alpha\text{-RuCl}_3$ below $T \simeq 80$ K (refs. 5,6) has been attributed to the excitations of a Kitaev spin liquid⁷. Similarly, the κ_{xy} signal observed in some frustrated magnets – in which there is no magnetic order down to the lowest temperatures – has been attributed to spin-related heat carriers⁸.

However, phonons can also generate a nonzero thermal Hall conductivity if some mechanism confers chirality to them. For instance, an intrinsic mechanism is the Berry curvature of phonon bands acquired from a magnetic environment⁹. In the ferrimagnetic insulator $\text{Fe}_2\text{Mo}_3\text{O}_8$, the large κ_{xy} signal is attributed to the strong spin-lattice coupling characteristic of multiferroic materials¹⁰. An extrinsic mechanism is the skew scattering of phonons by rare-earth impurities¹¹, as in the rare-earth garnet $\text{Tb}_3\text{Ga}_5\text{O}_{12}$ (refs.12,13). Recently, a large phononic κ_{xy} has been observed in the non-magnetic insulator SrTiO_3 (ref. 14). A proposed explanation involves the large ferroelectric susceptibility of this oxide insulator together with an extrinsic mechanism whereby phonons are scattered by the polar boundaries from the antiferrodistortive structural transition at 105 K (ref. 15). This interpretation is supported by the fact that κ_{xy} is negligible in the closely related material KTaO_3 (ref. 14), which remains cubic and free of structural domains.

In cuprates, a large negative κ_{xy} signal was observed at low temperature inside the pseudogap phase¹⁶, *i.e.* for dopings $p < p^*$, where p^* is the pseudogap critical doping¹⁷. Because it persists down to $p = 0$, in the Mott insulator state, this negative κ_{xy} cannot come from charge carriers, which are not mobile at $p = 0$. Therefore, it must come either from spin-related excitations (possibly topological, as in refs. 18,19) or from phonons (as in ref. 15). To distinguish between these two types of heat carriers, a simple approach was recently adopted: the thermal Hall conductivity was measured for a heat current along the c axis, normal to the CuO_2 planes, a direction in which only phonons move easily²⁰. In La_2CuO_4 , at $p = 0$, the thermal Hall signal was found to be just as large as for an in-plane heat current, *i.e.* $\kappa_{zy}(T) \simeq \kappa_{xy}(T)$ (ref. 21). This is compelling evidence that phonons are the heat carriers involved in the thermal Hall signal of this insulator. Moreover, it was found that this phonon Hall effect vanishes entirely immediately outside the pseudogap phase, *i.e.* $\kappa_{zy}(T) = 0$ at $p > p^*$, revealing that phonons only become chiral upon entering the pseudogap phase.

The question is: What makes the phonons in cuprates become chiral? In order to provide answers to this question, we have investigated two other cuprate Mott insulators, Nd_2CuO_4 and $\text{Sr}_2\text{CuO}_2\text{Cl}_2$, and find in both a large negative thermal Hall conductivity similar to that of La_2CuO_4 . While the three materials share the same fundamental characteristic of cuprates, namely they are a stack of single CuO_2 planes, there are significant differences between them (see Methods and Fig. 1). Our comparative study allows us to conclude that none of the distinguishing features – orthorhombicity, structural domain boundaries, apical oxygens, spin canting, noncollinear alignment of spins, nature of the cation – play a key role in causing the chirality. This points to a chiral mechanism associated with the coupling of phonons to the CuO_2 planes themselves.

RESULTS

Thermal Hall conductivity

In Fig. 2, we show our data for κ_{xx} and κ_{xy} in $\text{Sr}_2\text{CuO}_2\text{Cl}_2$ (sample A) and Nd_2CuO_4 . We see that as in La_2CuO_4 , both materials show a large negative thermal Hall signal. We also observe a certain field dependence of κ_{xx} , larger than the small one observed in La_2CuO_4 (ref. 16). In $\text{Sr}_2\text{CuO}_2\text{Cl}_2$, the field increases κ_{xx} slightly below $T \approx 20$ K. In Nd_2CuO_4 , the field decreases κ_{xx} below $T \approx 40$ K.

In Fig. 3, we compare the three cuprate Mott insulators. We observe that the curves of $-\kappa_{xy}$ vs T (right panels) are similar in shape, peaking at $T \approx 25$ K, a temperature close to that where κ_{xx} vs T peaks (left panels). At low temperature, κ_{xx} is dominated by phonons. Indeed, because there is a gap in the magnon spectrum of these antiferromagnets²², their contribution to κ_{xx} becomes negligible at low T compared to the phonon contribution. At $T = 35$ K, the magnon conductivity is only 2% of the measured κ_{xx} (ref. 20), and it rapidly becomes vanishingly small below that temperature. At $T = 20$ K, the magnitude of κ_{xx} is 8 times larger in Nd_2CuO_4 compared to $\text{Sr}_2\text{CuO}_2\text{Cl}_2$ (Fig. 3). So, phonons are a lot more conductive in Nd_2CuO_4 . We see from Figs. 3e and 3f that κ_{xy} is correspondingly (10 times) larger in Nd_2CuO_4 . This is strong evidence that phonons are the heat carriers responsible for the Hall response.

In Fig. 4, we plot the ratio $\kappa_{xy} / \kappa_{xx}$ vs T for the three materials. We see that not only is this ratio of similar magnitude in the three cuprates, but its temperature dependence is also very similar, growing with decreasing T to reach a maximal (negative) value at $T \approx 10 - 15$ K, where $|\kappa_{xy} / \kappa_{xx}| \approx 0.3 - 0.4$ % (at $H = 15$ T).

Having observed a large negative thermal Hall conductivity κ_{xy} in both Nd_2CuO_4 and $\text{Sr}_2\text{CuO}_2\text{Cl}_2$ that is very similar to that previously reported for La_2CuO_4 (*i.e.* of comparable magnitude when measured relative to κ_{xx}) allows us to draw several conclusions about the underlying mechanism for chirality in the cuprate Mott insulators.

Spin canting

It has been shown theoretically that in ferromagnetic or antiferromagnetic insulators, under certain conditions, magnons can have chirality and should give rise to a thermal Hall effect¹. In the collinear Néel antiferromagnetic order of La_2CuO_4 , no thermal Hall effect is expected theoretically, because of the so-called "no-go" theorem, which states that Néel order on a square lattice has zero chirality¹. However, if the spins of the Néel order cant out of the plane, as they do in La_2CuO_4 , then some Dzyaloshinskii-Moriya (DM) interaction develops and some chirality becomes possible. In this case, one could get a non-zero κ_{xy} signal, but it is expected to be much smaller than the measured κ_{xy} signal in La_2CuO_4 (ref. 23). Our data on Nd_2CuO_4 and $\text{Sr}_2\text{CuO}_2\text{Cl}_2$ completely eliminate this possibility, because a κ_{xy} signal of similar or larger magnitude is found in these materials for which there is no canting of spins out of the plane (see Methods), and so no DM interaction. We conclude that magnons are not responsible for the thermal Hall effect in cuprate Mott insulators. This conclusion is consistent with the fact that in La_2CuO_4 a large κ_{xy} signal persists down to temperatures well below the smallest magnon gap (of magnitude 26 K (ref. 22)) and up in doping well above the critical doping ($p \approx 0.02$) for the suppression of Néel order in, $\text{La}_{2-x}\text{Sr}_x\text{CuO}_4$ (ref. 16).

As for a phonon scenario whereby phonons would acquire chirality through their coupling to spins, spin canting also appears to be unimportant.

Let us now consider two mechanisms known to confer chirality to phonons in other materials – skew scattering off rare-earth impurities and scattering off structural domain boundaries – and show that neither is relevant to cuprates.

Nature of cation

The initial observation of a phonon thermal Hall effect, in the garnet $\text{Tb}_3\text{Ga}_5\text{O}_{12}$ (refs. 12,13), has been attributed to the skew scattering of phonons by superstoichiometric Tb^{3+} ions¹¹. This extrinsic mechanism depends crucially on the details of the crystal-field levels of the rare-earth ion. A different rare-earth ion will in general produce skew scattering of a very different strength. The fact that the ratio $\kappa_{xy} / \kappa_{xx}$ is the same in all

three cuprates considered here is compelling evidence that the underlying mechanism does not depend on the nature of the particular cation, whether La, Sr or Nd.

Note also that strong skew scattering by rare-earth impurities shows up as a major reduction in κ_{xx} (ref. 24). In $\text{Tb}_3\text{Ga}_5\text{O}_{12}$, 2% of Tb^{3+} impurities gives rise to both a finite κ_{xy} signal from phonons (whose magnitude is given in Table I) and a 5-fold reduction in κ_{xx} (ref.13), whose value at $T=15$ K is then only $\kappa_{xx}=1.2$ W/Km (ref. 11). In the pyrochlore oxide $\text{Tb}_2\text{Ti}_2\text{O}_7$, a frustrated magnet with a sizable thermal Hall effect⁸ (Table I), κ_{xx} is massively reduced compared to $\text{Y}_2\text{Ti}_2\text{O}_7$, by a factor 15 at $T=15$ K ($H=0$) (ref. 25), pointing again to strong scattering of phonons by Tb^{3+} ions. (Note that the thermal Hall effect in $\text{Tb}_2\text{Ti}_2\text{O}_7$ has recently been attributed to phonons²⁶.) By comparison, the thermal conductivity in the cuprate Mott insulators is an order of magnitude larger (see Table I), evidence that no strong skew scattering is at play $\kappa_{xx} = 10$ W/Km in La_2CuO_4 , 45 W/Km in Nd_2CuO_4 , and 6 W/Km in $\text{Sr}_2\text{CuO}_2\text{Cl}_2$, at $T=15$ K ($H=15$ T; Fig. 3). We conclude that skew scattering of phonons by superstoichiometric cation atoms is not the mechanism that confers chirality to phonons in cuprates.

Structural domains

In the nonmagnetic insulator SrTiO_3 , a negative thermal Hall conductivity was recently observed¹⁴, with a magnitude comparable to that of the three cuprate Mott insulators (see Table I). There is little doubt that the thermal Hall effect in SrTiO_3 is due to phonons. Importantly, the κ_{xy} signal in the closely related oxide KTaO_3 is 30 times smaller (and of opposite sign)¹⁴ (Table I). The key difference between the two materials is that SrTiO_3 undergoes an antiferrodistortive structural transition at 105 K, whereas KTaO_3 remains cubic down to $T \approx 0$ K. The authors of the study on those two materials conclude that the large signal in SrTiO_3 is linked to the structural domain boundaries that exist below 105 K (ref. 14), although the precise mechanism whereby these confer chirality to phonons is still unclear. Our comparative study of the three cuprates allows us to rule out a similar role for structural domains. Indeed, whereas La_2CuO_4 undergoes a structural transition to an orthorhombic phase below 530 K, Nd_2CuO_4 and $\text{Sr}_2\text{CuO}_2\text{Cl}_2$ both remain

tetragonal down to $T \approx 0$ K, and yet all three have a similar thermal Hall effect, in both T dependence (Fig. 3) and magnitude – relative to κ_{xx} (Fig. 4 and Table I).

Magnetostructural domains

Because the collinear spin order in $\text{Sr}_2\text{CuO}_2\text{Cl}_2$ breaks the 4-fold symmetry of the lattice, there will be antiferromagnetic domains below T_N and these will in principle be accompanied by an orthorhombic distortion of the tetragonal lattice aligned with the moment direction in each domain. To investigate the possible effect of these putative structural distortions, we have measured κ_{xy} in the same sample of $\text{Sr}_2\text{CuO}_2\text{Cl}_2$ (sample B) under three different conditions: 1) for a field $H = 10.6$ T applied along the c axis; 2) for a field $H = 15$ T applied at an angle of 45 degrees from the c axis (whose components normal and parallel to the CuO_2 planes are both 10.6 T), applied at $T = 2$ K (zero-field cooling); 3) same as for 2), but applied at $T = 300$ K $> T_N$ (in-field cooling). In the latter in-field cooling condition, the in-plane component of the field (of magnitude 10.6 T) applied at $T > T_N$ will ensure that a single antiferromagnetic domain is present below T_N . (We expect the in-plane field needed to create a mono-domain to be approximately 5 T, as verified in $\text{YBa}_2\text{Cu}_3\text{O}_6$ (ref. 27).) Comparing conditions 2) and 3) amounts to comparing a multi-domain sample vs a mono-domain sample.

The results of this study are displayed in Fig. 5. We see that κ_{xy} is identical in the three situations, within error bars. So, magnetic domains in $\text{Sr}_2\text{CuO}_2\text{Cl}_2$, and any associated structural distortions, do not influence the thermal Hall response. Note that the noncollinear order in Nd_2CuO_4 does not break the 4-fold symmetry of the lattice, so here no magnetic domains are expected.

We conclude that structural (or magnetostructural) domains are not the mechanism that confers chirality to phonons in cuprates. Moreover, the thermal Hall conductivity of cuprates is independent of whether the system has orthorhombic or tetragonal symmetry, or whether there are apical oxygens in the structure or not.

In summary, our results show that the cuprate Mott insulators Nd_2CuO_4 and $\text{Sr}_2\text{CuO}_2\text{Cl}_2$ exhibit a large negative thermal Hall conductivity κ_{xy} very similar to that found in La_2CuO_4 . The fact that the magnitude of κ_{xy} scales with the magnitude of the phonon-dominated κ_{xx} as the latter varies by a factor 10 between $\text{Sr}_2\text{CuO}_2\text{Cl}_2$ and Nd_2CuO_4 is further evidence in favor of phonons as the carriers of heat responsible for the thermal Hall effect in these materials. Given the different crystal structures and cations involved in those three materials, the similarity in $\kappa_{xy} / \kappa_{xx}$ allows us to rule out two extrinsic mechanisms of phonon chirality proposed for other oxides, namely the scattering off rare-earth impurities – invoked for $\text{Tb}_3\text{Gd}_5\text{O}_{12}$ – and the scattering off structural domain boundaries – invoked for SrTiO_3 . This suggests that phonon chirality in the cuprates comes from an intrinsic coupling of phonons to their environment.

DISCUSSION

Phonons can acquire chirality through a coupling to their intrinsic environment (see, *e.g.*, ref. 9). This could involve a coupling to charge or a coupling to spin, for example. In ref. 15, a flexoelectric coupling of phonons to their charge environment was shown to generate a Hall response. However, even in the nearly ferroelectric insulator SrTiO_3 , where the electric polarizability is exceptionally large, this intrinsic mechanism is estimated to be much too small. The inclusion of some additional, extrinsic, scattering mechanism – possibly structural domain boundaries – is deemed necessary. Applied to cuprates, the intrinsic flexoelectric coupling is certainly much too small. It is not clear what extrinsic mechanism could be added to make this mechanism strong enough to account for the observed data in the cuprate Mott insulators.

In multiferroic materials like $\text{Fe}_2\text{Mo}_3\text{O}_8$, a large κ_{xy} signal is observed even in the paramagnetic phase¹⁰, where $\kappa_{xy} / \kappa_{xx} \approx 0.5\%$ (at $T = 65$ K and $H = 14$ T) (Table I). This is attributed to a strong spin-lattice coupling. In cuprates, a coupling of phonons to spins in their environment should be investigated as a possible source of chirality.

Another avenue of investigation for cuprates is the possibility that they harbour exotic chiral excitations, like spinons^{18,19} that could couple to phonons. Such a coupling has recently been considered for the case of Majorana fermions in a Kitaev spin liquid²⁸.

In a scenario of phonons coupled to their environment, there could be two relevant regimes of temperature, namely above and below the peak in κ_{xy} vs T , so roughly above 25 K and below 15 K, respectively (Fig. 3). At temperatures above the peak, it has been shown that if the heat carriers have Berry curvature they would be expected to exhibit a characteristic exponential dependence, namely $\kappa_{xy}/T \propto \exp(-T/T_0)$ (ref. 29). In Fig. 6, we fit our data on $\text{Sr}_2\text{CuO}_2\text{Cl}_2$ and Nd_2CuO_4 to that form and find a good fit over the intermediate temperature range from 30 K to 100 K. An equally good fit is found for La_2CuO_4 (ref. 21). Whether this implies that phonons acquire a Berry curvature through their coupling to the environment remains to be determined. At low temperature, we would expect phonons to eventually decouple from their environment, whether that be spins or other excitations of electronic origin. The temperature below which they do so would shed light on the nature of that coupling. In Fig. 4, we see that upon cooling below 10 K, $|\kappa_{xy}|$ in $\text{Sr}_2\text{CuO}_2\text{Cl}_2$ falls more rapidly to zero than κ_{xx} does. (Our current data on Nd_2CuO_4 and La_2CuO_4 do not allow us to explore the regime below 10 K.) In Fig. 7, we zoom on the low- T regime in $\text{Sr}_2\text{CuO}_2\text{Cl}_2$. We see that whereas κ_{xx}/T^3 rises monotonically as $T \rightarrow 0$, κ_{xy}/T^3 drops rapidly towards zero, starting roughly at 5 K. We identify 5 K as the approximate decoupling temperature between acoustic phonons and their chiral environment.

It is instructive to compare our data on undoped cuprates to prior data on hole-doped cuprates. At a doping $p = 0.24$, in both Nd-LSCO and Eu-LSCO, the thermal Hall signal coming from phonons – as opposed to charged carriers – is zero²¹ (Table I). It only becomes nonzero when the doping is reduced below the critical doping for the pseudogap phase, *i.e.* when $p < p^*$ ($p^* = 0.23$). The magnitude of the κ_{xy} is relatively constant p^* down to $p = 0$ when measured relative to κ_{xx} (see Table I), and the sign is negative throughout. This continuity suggests that the same chiral mechanism is at play in the Mott insulator and within the pseudogap phase.

Moreover, because the phononic κ_{xy} signal in Nd-LSCO goes from zero at $p = 0.24$ to its full value at $p = 0.21$, rising abruptly upon crossing below p^* , this chiral mechanism must be an intrinsic property of the pseudogap phase – since there is no change in the crystal structure²¹ and little change in the amount of impurity scattering between $p = 0.24$ and $p = 0.21$. This is consistent with our finding that structural domains and cation impurities are unimportant, and it extends the argument to all other defects and impurities, *e.g.* oxygen vacancies, all of which are essentially unchanged between $p = 0.24$ and $p = 0.21$.

A possible mechanism is the coupling of phonons to short-range antiferromagnetic correlations. Experimental evidence for such correlations includes the Fermi-surface transformation across p^* observed by angle-dependent magnetoresistance (ADMR)³⁰ and the drop-in carrier density across p^* observed in electrical Hall effect^{31,32,33}, both consistent with spin modulations with a wavevector $Q = (\pi, \pi)$. Solutions of the Hubbard model in the paramagnetic state find that, in doped Mott insulators such as the cuprates, local moments^{34,35} persist all the way from half-filling up to a critical doping where the pseudogap disappears^{36,37,38}. In calculations within the pseudogap phase, superexchange between local moments naturally favors short-range antiferromagnetic^{39,40,41} or singlet correlations^{34,35}.

In such a scenario, the question becomes: How can the coupling of phonons to spins make these phonons chiral (in the presence of a magnetic field)?

ACKNOWLEDGMENTS

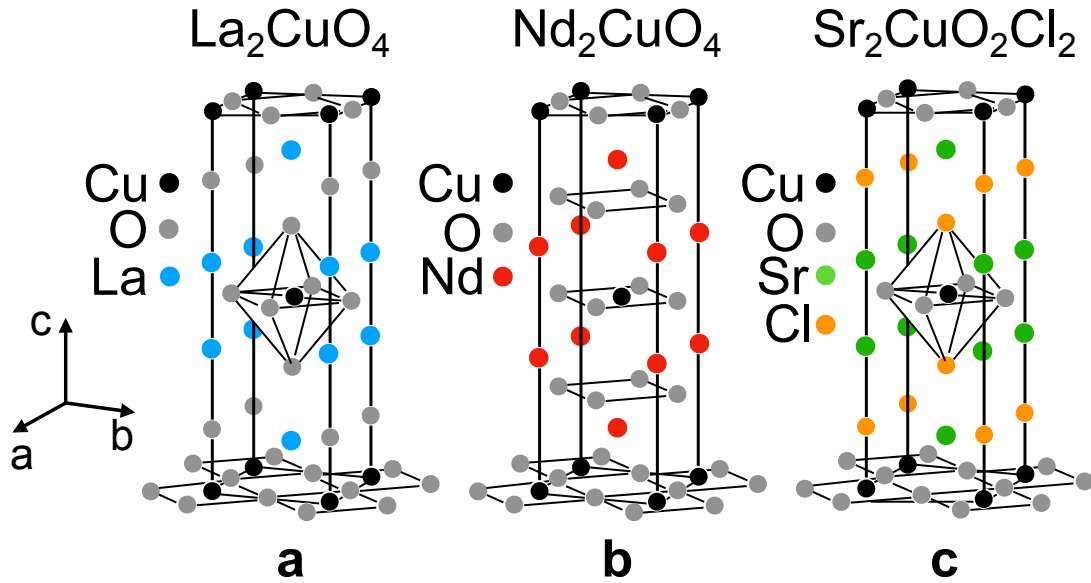
L.T. acknowledges support from the Canadian Institute for Advanced Research (CIFAR) as a CIFAR Fellow and funding from the Natural Sciences and Engineering Research Council of Canada (NSERC; PIN: 123817), the Fonds de recherche du Québec - Nature et Technologies (FRQNT), the Canada Foundation for Innovation (CFI), and a Canada Research Chair. This research was undertaken thanks in part to funding from the Canada Research Excellence Fund. Part of this work was funded by the Gordon and Betty Moore Foundations EPIQS Initiative (Grant GBMF5306 to L.T.). This work was also supported by the National Natural Science Foundation of China (11888101 and 11534010).

AUTHOR CONTRIBUTIONS

M.-E.B., G.G., S.B., A.A., E.L. and A.G. performed the thermal Hall measurements.

M.-E.B., G.G., S.B., A.A. and E.L. analyzed the results. M.D. performed the X-ray diffraction measurements. C.H.W. and X.H.C. grew the Nd_2CuO_4 crystal. R.L., W.N.H. and D. A. B. grew the $\text{Sr}_2\text{CuO}_2\text{Cl}_2$ crystals. M.-E.B., G.G. and L.T. wrote the manuscript, in consultation with all authors. L.T. supervised the project.

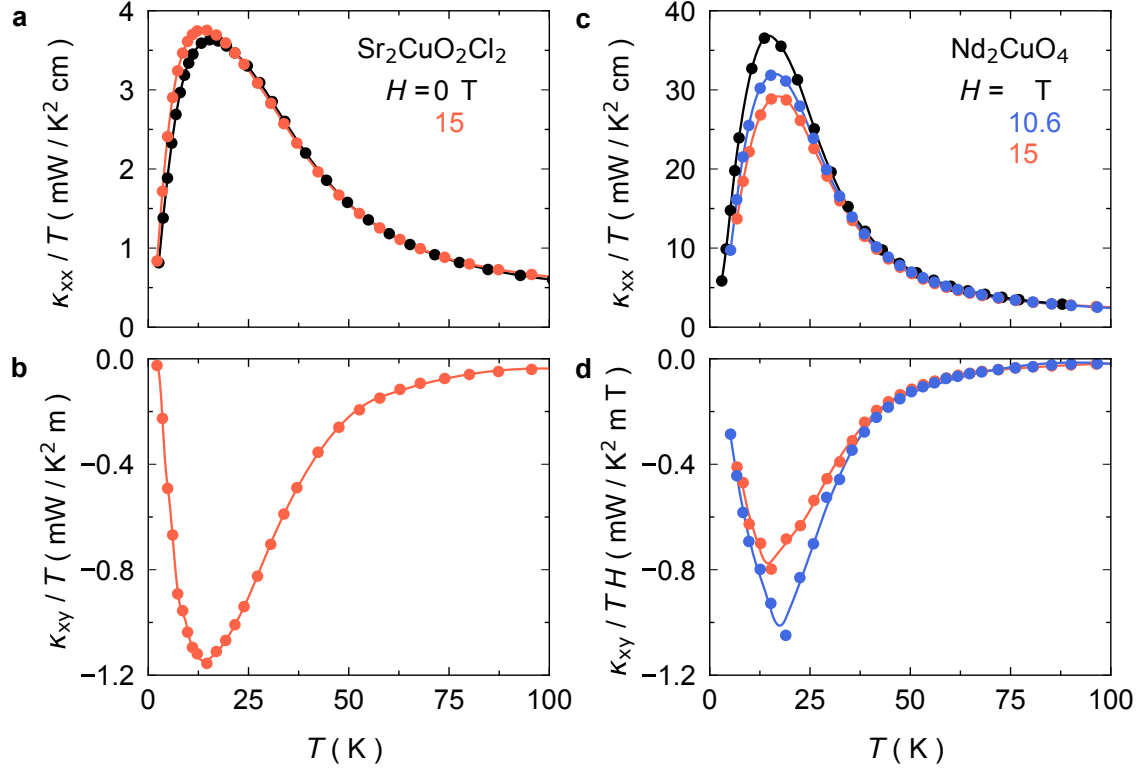
Fig. 1 | Crystal structure of La_2CuO_4 , Nd_2CuO_4 and $\text{Sr}_2\text{CuO}_2\text{Cl}_2$.



Sketch of the crystal structure of the three single-layer cuprate Mott insulators compared in the present study: **a)** La_2CuO_4 ; **b)** Nd_2CuO_4 ; **c)** $\text{Sr}_2\text{CuO}_2\text{Cl}_2$.

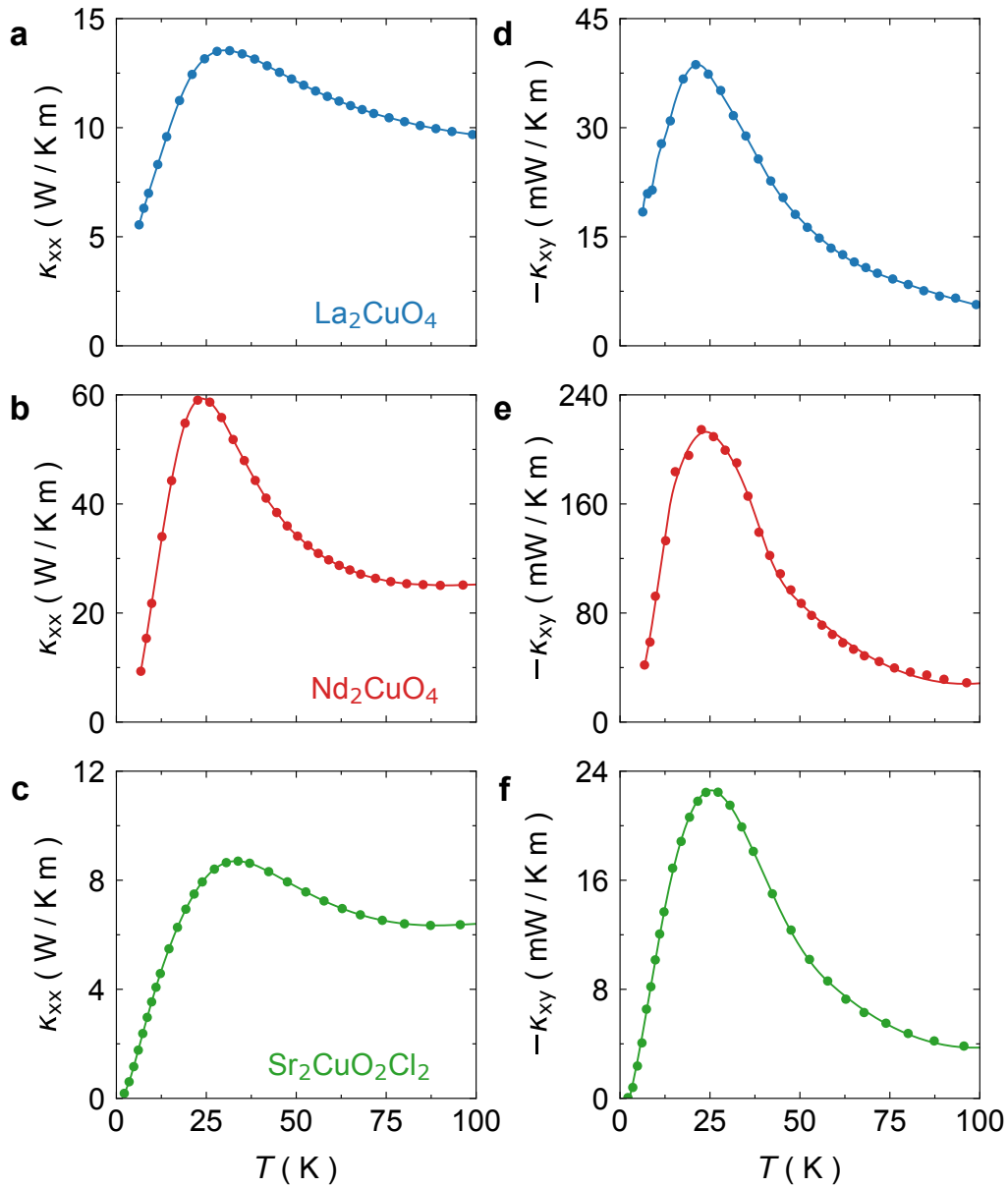
Note that the small orthorhombic distortion in La_2CuO_4 below 530 K is not shown here, nor is the tilt in the oxygen octahedra surrounding the Cu atoms.

Fig. 2 | Thermal transport in $\text{Sr}_2\text{CuO}_2\text{Cl}_2$ and Nd_2CuO_4 .



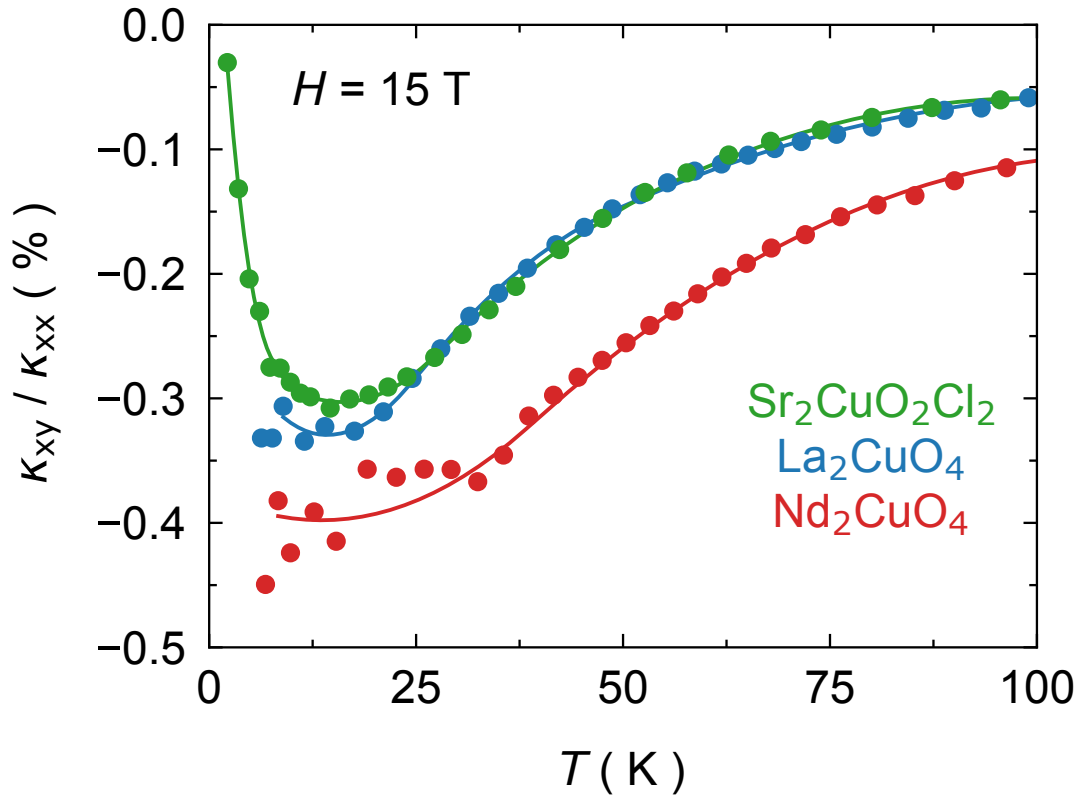
a Thermal conductivity of $\text{Sr}_2\text{CuO}_2\text{Cl}_2$ (sample A) in zero field ($H = 0$; black) and in a field of 15 T applied parallel to the c -axis (light-red), plotted as κ_{xx}/T vs T . The field is seen to increase κ_{xx} slightly at low temperature. **b** Thermal Hall conductivity of $\text{Sr}_2\text{CuO}_2\text{Cl}_2$ (same sample) in a field of 15 T applied parallel to the c -axis, plotted as κ_{xy}/T vs T . **c** Thermal conductivity of Nd_2CuO_4 , plotted as κ_{xx}/T vs T , for three values of the magnetic field applied parallel to the c -axis: $H = 0$ (black); $H = 10.6$ T (blue); $H = 15$ T (light-red). In this case, the field is seen to decrease κ_{xx} at low temperature. **d** Thermal Hall conductivity of Nd_2CuO_4 , plotted as $\kappa_{xy}/(TH)$ vs T , for two values of the magnetic field applied parallel to the c axis: $H = 10.6$ T (blue); $H = 15$ T (light-red). The Hall conductivity κ_{xy} is seen to be sublinear in H at low T and linear in H at high T ($T > 50$ K). All lines are a guide to the eye.

Fig. 3 | Thermal Hall conductivity in the three Mott insulators.



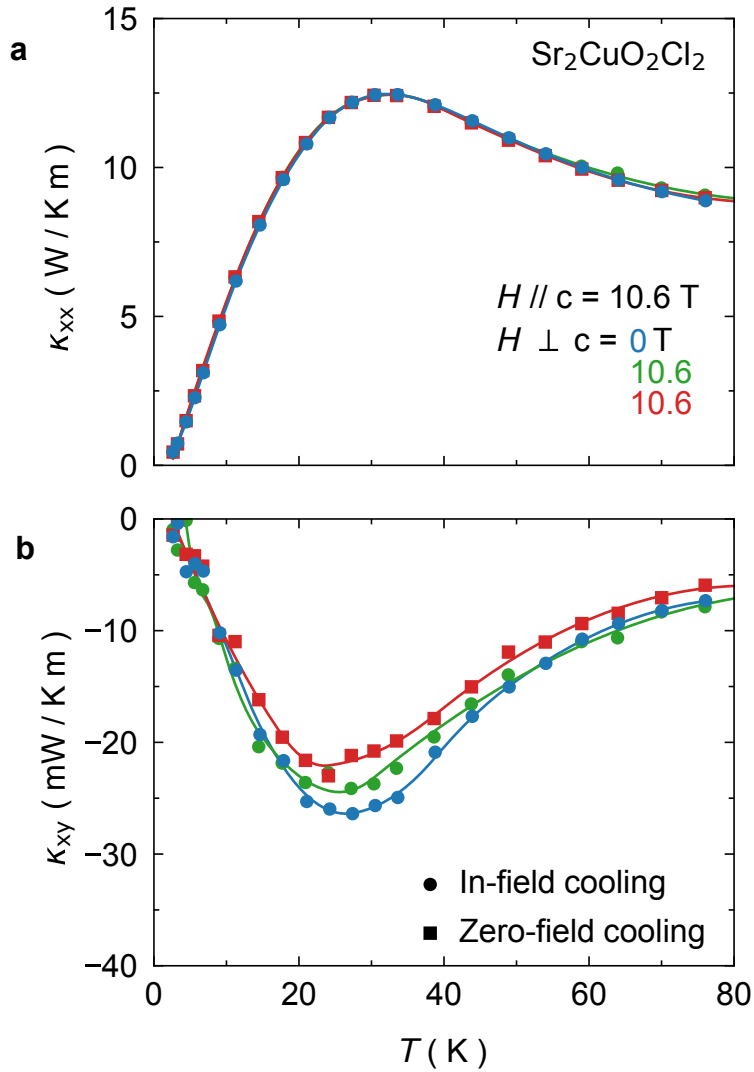
Left panels: Thermal conductivity of the three cuprate Mott insulators, plotted as κ_{xx} vs T : **a)** La_2CuO_4 ; **b)** Nd_2CuO_4 ; **c)** $\text{Sr}_2\text{CuO}_2\text{Cl}_2$. Right panels: Corresponding thermal Hall conductivity, plotted as $-\kappa_{xy}$ vs T : **d)** La_2CuO_4 ; **e)** Nd_2CuO_4 ; **f)** $\text{Sr}_2\text{CuO}_2\text{Cl}_2$. All data shown in this figure were taken in a field of 15 T (along the c axis).

Fig. 4 | Ratio of κ_{xy} over κ_{xx} .



Ratio of κ_{xy} over κ_{xx} in the three cuprate Mott insulators (expressed in %), measured in a field of 15 T applied parallel to the c-axis: $\text{Sr}_2\text{CuO}_2\text{Cl}_2$ (green); La_2CuO_4 (blue); Nd_2CuO_4 (red). All lines are a guide to the eye. We see that despite a factor 10 in the magnitude of κ_{xy} between $\text{Sr}_2\text{CuO}_2\text{Cl}_2$ and Nd_2CuO_4 (Fig. 2), the ratio $\kappa_{xy} / \kappa_{xx}$ is very similar in magnitude for all three cuprates.

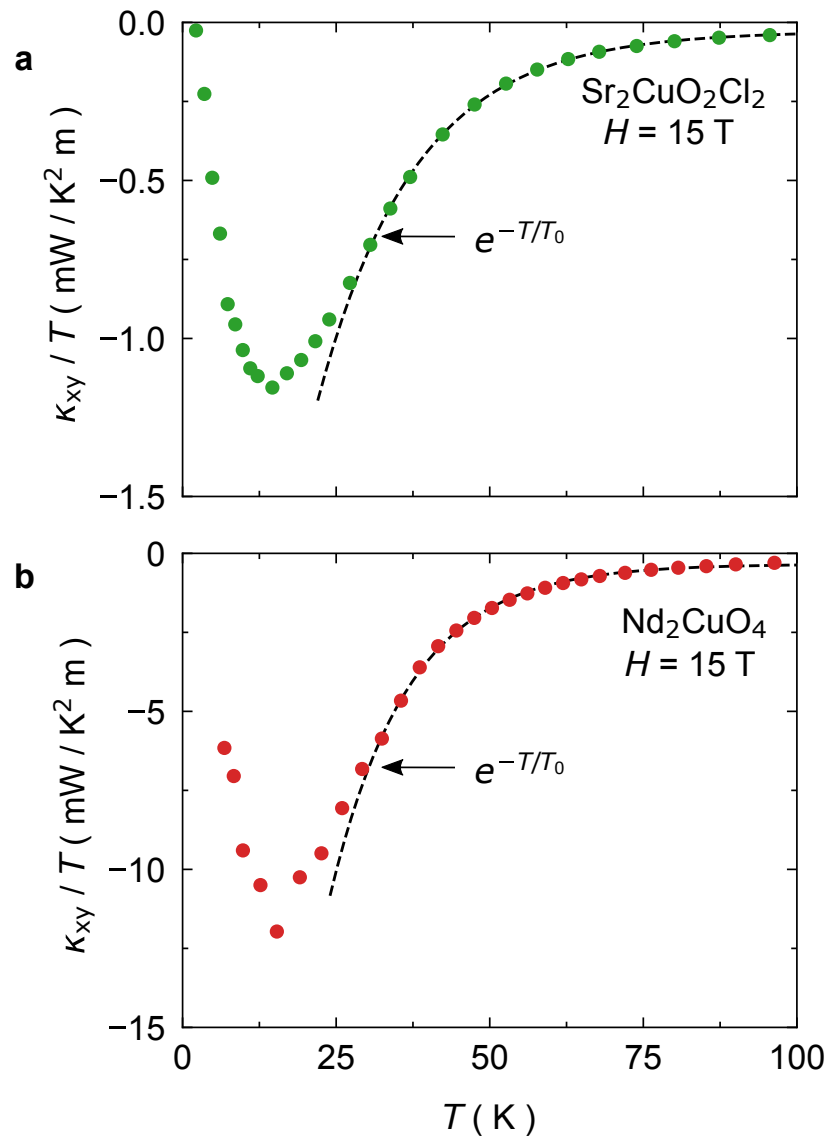
Fig. 5 | Effect of magnetostructural domains in $\text{Sr}_2\text{CuO}_2\text{Cl}_2$.



Thermal transport of our sample B of $\text{Sr}_2\text{CuO}_2\text{Cl}_2$ or a heat current $J // a$, measured as a function of increasing temperature from $T = 2$ K up to 80 K, in three different conditions: 1) for a field $H = 10.6$ T along the c axis, applied at $T = 300$ K (blue circles); 2) for a field $H = 15$ T at 45 degrees from the c axis (meaning equal in-plane and out-of-plane fields, *i.e.* $H \perp c = H // c = 10.6$ T), applied at $T = 2$ K (zero-field cooling; red squares); 3) for a field $H = 15$ T at

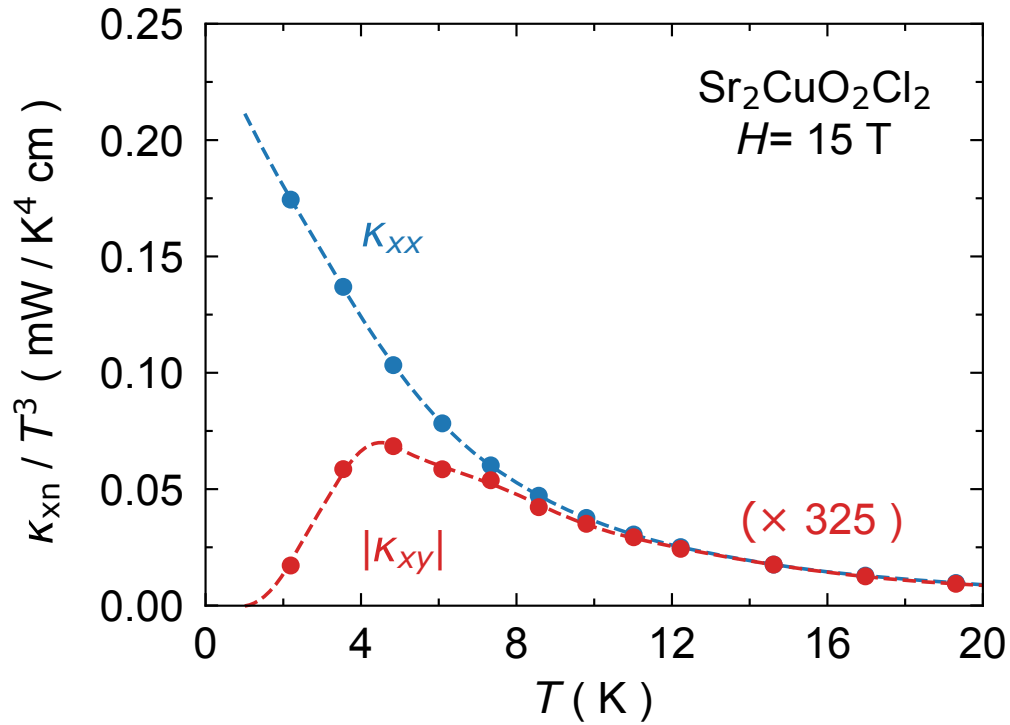
45 degrees from the c axis, applied at $T = 300$ K (in-field cooling; green circles). All lines are a guide to the eye. In conditions 1) and 2), we expect that multiple orthorhombic magnetostructural domains and associated boundaries exist below $T_N = 270$ K. Condition 3) – in-field cooling in the presence of an in-plane field of 10.6 T – ensures that a single antiferromagnetic domain exists when magnetic order sets in below T_N , and so there should be no, or very few, structural domain boundaries in that case. **a** Thermal conductivity κ_{xx} vs T . There is no detectable difference between the three curves, showing that the presence of magnetostructural domains has negligible impact on the phonon thermal conductivity. **b** Thermal Hall conductivity κ_{xy} vs T . Within error bars, there is no significant difference between the three curves, demonstrating that magnetostructural domains do not play a significant role in generating the thermal Hall effect in $\text{Sr}_2\text{CuO}_2\text{Cl}_2$.

Fig. 6 | Phenomenological fit to the phonon thermal Hall conductivity.



Thermal Hall conductivity, plotted as κ_{xy}/T vs T in **a)** $\text{Sr}_2\text{CuO}_2\text{Cl}_2$ (sample A) and **b)** Nd_2CuO_4 . The data are fit to the phenomenological expression $\kappa_{xy}/T = A \exp(-T/T_0) + C$ from ref. 29. The fit interval is 30 K to 100 K. The resulting fit parameters are **(a)** $A = -5 \text{ mW}/\text{K}^2 \text{cm}$, $C = -0.03 \text{ mW}/\text{K}^2 \text{cm}$, $T_0 = 16 \text{ K}$; **(b)** $A = -67 \text{ mW}/\text{K}^2 \text{cm}$, $C = -0.3 \text{ mW}/\text{K}^2 \text{cm}$, $T_0 = 12 \text{ K}$.

Fig. 7 | Low-temperature regime in $\text{Sr}_2\text{CuO}_2\text{Cl}_2$.



Thermal conductivity κ_{xx} and thermal Hall conductivity κ_{xy} of $\text{Sr}_2\text{CuO}_2\text{Cl}_2$ (sample A), plotted as κ_{xx} / T^3 (blue) and $-\kappa_{xy} / T^3$ (red) vs T . The dashed lines are a guide to the eye. Note that the κ_{xy} data are multiplied by a factor 325, to compare it more easily with κ_{xx} , using only one y-axis scale.

Table I | Thermal Hall conductivity in various oxide insulators.

Material	Doping	κ_{xy}	κ_{xx}	$ \kappa_{xy} / \kappa_{xx} $	T	H	Reference
		mW / K m	W / K m	%	K	T	
Nd ₂ CuO ₄	0.00	-212.5	58.3	0.37	22	15	This work
Sr ₂ CuO ₂ Cl ₂	0.00	-22.3	8.2	0.26	25	15	This work
La ₂ CuO ₄	0.00	-38.6	12.4	0.30	20	12	16
La ₂ CuO ₄ ($J // c$)	0.00	-30.0	16	0.2	20	15	21
LSCO	0.06	-30.0	5.1	0.58	15	15	16
Eu-LSCO	0.08	-13.2	4.5	0.29	15	15	16
Nd-LSCO ($J // c$)	0.21	-14.0	2.9	0.48	20	15	21
Nd-LSCO ($J // c$)	0.24	0	1.2	0	20	15	21
Eu-LSCO ($J // c$)	0.24	0	1.2	0	20	15	21
Lu ₂ V ₂ O ₇		+1.0	-	0.14	50	0.1	3
Tb ₃ Ga ₅ O ₁₂		+0.02 ^a	0.2	0.01	5	3	13
Tb ₂ Ti ₂ O ₇		+1.2	0.27	0.44	15	12	8
Y ₂ Ti ₂ O ₇		0	18	0	15	8	8,25
(Tb _{0.3} Y _{0.7}) ₂ Ti ₂ O ₇		+3.8	1.0	0.38	15	12	26
SrTiO ₃		-80	36	0.20	20	12	14
KTaO ₃		+2	30	0.007	30	12	14

^a Expected to be 10 times larger at $T = 20$ K and $H = 15$ T.

The magnitude and sign of κ_{xy} are given for a temperature T and magnetic field H as indicated. The quoted values are typically the largest absolute values for a field of 15 T or so. The value of κ_{xx} at the same T and H is also given, as is the corresponding ratio $|\kappa_{xy} / \kappa_{xx}|$. The first group of materials is cuprates, including the three undoped Mott insulators studied here (top) and some hole-doped

cuprates, whose doping p is indicated in the second column. At high doping ($p > 0.2$), the samples are not insulating but metallic and so we quote here the thermal transport coefficients for a heat current normal to the CuO_2 planes ($J // c$) which contain only the phonon contribution to heat transport. The second group consists of one material, the ferromagnet $\text{Lu}_2\text{V}_2\text{O}_7$, whose κ_{xy} signal is due to magnons. The third group consists of insulating materials with no magnetic order. It includes four pyrochlore oxides with Tb and / or Y ions, whose magnetism is either frustrated (Tb) or absent (Y), and two non-magnetic oxides (SrTiO_3 and KTaO_3). The last group consists of the multiferroic material $\text{Fe}_2\text{Mo}_3\text{O}_8$, which has ferrimagnetic order below 45 K. Here we quote values above that temperature, in the paramagnetic state at 65 K.

METHODS

CRYSTAL STRUCTURES

La₂CuO₄

La₂CuO₄ is the parent compound of the most widely studied family of single-layer cuprates, La_{2-x}Sr_xCuO₄. In La₂CuO₄, there is an (apical) oxygen atom above the Cu atom, thereby forming an octahedron of O atoms around Cu (Fig. 1). Upon cooling from high temperature, La₂CuO₄ goes from a tetragonal (I4/mmm) structure to an orthorhombic (Cmca) structure at 530 K (ref. 42), wherein the octahedra are tilted (the orthorhombic distortion and associated tilt are not shown in Fig. 1). This means that unless they are deliberately detwinned by application of uniaxial stress, crystals of La₂CuO₄ will be full of orthorhombic structural domains (twins) whose boundaries can in principle scatter phonons. (The samples of La₂CuO₄ studied in refs. 16,21 were twinned.) Below $T_N = 270$ K, the Cu spins order into a collinear antiferromagnetic arrangement, whereby all alternating moments point along the same direction ([110]) within every CuO₂ plane inside a given orthorhombic domain. The tilting of the oxygen octahedra causes a slight canting of the spins out of the CuO₂ plane (by 0.17°) (ref. 43), thereby producing a Dzyaloshinskii-Moriya (DM) interaction that could, in principle, be a source of chirality.

Nd₂CuO₄

Nd₂CuO₄ is the parent compound of the electron-doped family of cuprates Nd_{2-x}Ce_xCuO₄. Unlike La₂CuO₄, it does not undergo any structural transition and remains tetragonal down to $T = 0$. A significant difference from La₂CuO₄ is the absence of apical oxygens, so that Cu atoms in Nd₂CuO₄ are not surrounded by oxygen octahedra (Fig. 1). So, in Nd₂CuO₄ there are no structural domain boundaries and no spin canting.

Magnetically, Nd₂CuO₄ differs from La₂CuO₄ in two ways: there is a large moment on the Nd³⁺ ions and the Cu spins adopt a noncollinear antiferromagnetic order⁴⁴. Below $T_N = 255$ K, the spins of the Cu²⁺ ions order antiferromagnetically along the Cu-O bond ([100]). This breaks the four-fold symmetry within a single CuO₂ plane. However, in the next CuO₂ plane along the c axis, the same spin configuration is rotated by 90°, thereby

restoring the four-fold symmetry of the entire system. This noncollinear magnetic structure therefore preserves the tetragonal symmetry of the crystal.

Sr₂CuO₂Cl₂

Sr₂CuO₂Cl₂ has the same crystal structure as tetragonal La₂CuO₄ ($T > 530$ K), with La replaced by Sr and the apical O replaced by Cl (Fig. 1). Unlike La₂CuO₄, it remains tetragonal down to low temperature and its octahedra shows no sign of tilting^{45,46,47}. So here again there are no structural domain boundaries and no spin canting. Sr₂CuO₂Cl₂ develops collinear antiferromagnetic order below $T_N = 250$ K, with a magnetic structure similar to that of La₂CuO₄ (moments along [110]), except with no spin canting out of the plane⁴⁶. It remains in the same magnetic phase down to at least $T = 10$ K (ref. 46).

SAMPLES

Our single crystal of Nd₂CuO₄ was grown at the University of Science and Technology of China by a standard flux method, annealed in helium for 10 h at 900°C, and cut in the shape of rectangular platelets with dimensions 0.50 x 0.69 x 0.066 mm³ (length between contacts × width × thickness in the c direction). Contacts were made with silver epoxy, diffused at 500°C for 1 h. The thermal conductivity κ_{xx} of similar samples was studied in detail at low temperature ($T < 20$ K) (refs. 48,49). Single crystals of Sr₂CuO₂Cl₂ were grown at the University of British Columbia using a flux-grown method. Here we report data on two samples (labeled A and B), cut in the shape of rectangular platelets with dimensions 0.6 x 0.11 x 0.03 mm³. Contacts we made using silver paint. In all cases, the heat current was made to flow along the a axis of the tetragonal structure.

MEASUREMENTS

The thermal conductivity κ_{xx} was measured applying a heat current J_x within the CuO₂ plane, generating a longitudinal temperature difference $\Delta T_x = T^+ - T^-$. The thermal conductivity along the x axis is given by $\kappa_{xx} = (J_x / \Delta T_x) (L / w t)$, where L is the distance between T^+ and T^- , w is the width of the sample and t its thickness. By applying a magnetic field along the c -axis of the crystal, normal to the CuO₂ planes, a transverse

temperature gradient, ΔT_y , was generated (see inset of Supplementary Figure 1). The thermal Hall conductivity is defined as

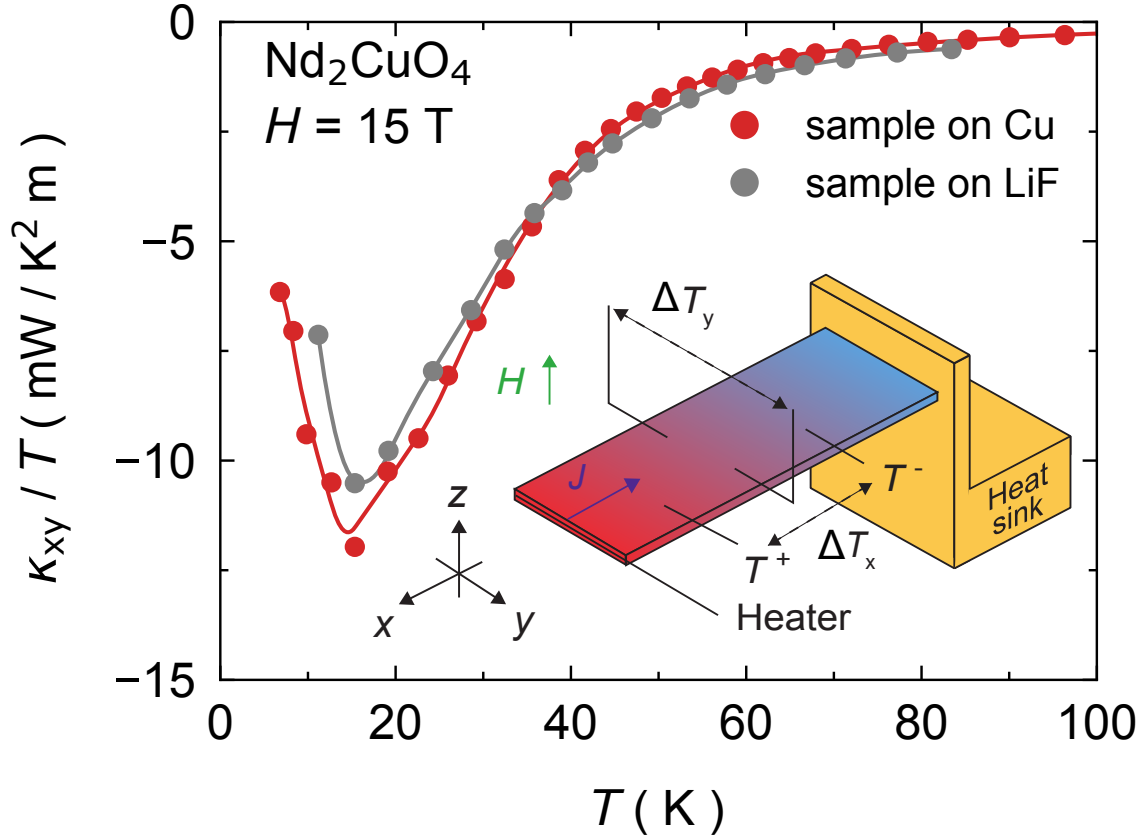
$$\kappa_{xx} = -\kappa_{yy} (\Delta T_x / \Delta T_y) (L / w)$$

where κ_{xy} is the longitudinal thermal conductivity along the y axis. Due to the tetragonal structure of our samples, we can take $\kappa_{xx} = \kappa_{yy}$.

The measurements were made with a steady-state method as a function of temperature, using differential type-E thermocouples for ΔT_x and ΔT_y (see inset of Supplementary Figure 1). This method consists in keeping the sample in a fixed magnetic field H and changing its temperature in discrete steps, typically of 2-3 K. At each fixed temperature, the background value of the thermocouple that measures ΔT_y is recorded before sending heat J to the sample. Once the sample is entirely in equilibrium, we measure $\Delta T_y (H)$. Here, the voltage (heat-off) background in the thermocouple is carefully subtracted from the heat-on signal of the thermocouple to give the correct $\Delta T_y (H)$. Once the entire temperature range is covered, say from 10 K to 100 K, the field direction is reversed to $-H$. The same procedure is now applied for these negative values of field. We then define $\Delta T_y (H) = [\Delta T_y (T, H) - \Delta T_y (T, -H)] / 2$, thereby removing any symmetric contamination of the signal coming from the longitudinal thermal gradient and the possible misalignment of transverse contacts.

The heat current along the x axis is generated by a heater stuck at one end of the sample. The other end is glued to a block that serves as a heat sink (see inset of Supplementary Figure 1). For the data reported here (and in refs. 16,21), this block was made of copper. To confirm that the Hall response of copper in a field does not contaminate the Hall response coming from the sample, we performed the same measurement twice, once with the copper block (using metallic contacts made with Ag paint) and then with a block made of the insulator LiF (using insulating contacts made with GE varnish), using the same sample of Nd_2CuO_4 in both cases. The results are shown in Supplementary Figure 1; we see that the same κ_{xy} curve is obtained with the two setups. We conclude that using copper for the heat sink does not lead to any detectable contamination of the thermal Hall signal.

Supplementary Figure 1 | Thermal Hall conductivity measurement



Thermal Hall conductivity κ_{xy} of our Nd_2CuO_4 sample, measured in a magnetic field $H = 15 \text{ T}$, plotted as κ_{xy}/T vs T . Two measurements were carried out: one with the heat sink made of copper (yellow data points) and the other one with the heat sink made of LiF (gray data points). Inset: Sketch of the measurement setup. One end of the thin sample is glued to a heat sink, while the other end is heated using a resistive heater attached to the sample by a silver wire. The heat current J generates a longitudinal temperature difference ΔT_x , both along the length of the sample (x direction). A magnetic field H applied along the z direction produces a transverse temperature difference ΔT_y between the two sides of the sample, along the y direction.

-
- ¹ Katsura, H., Nagaosa, N. & Lee, P. A. Theory of the thermal Hall effect in quantum magnets. *Phys. Rev. Lett.* **104**, 066403 (2010).
- ² Lee, H., Han, J. H. & Lee, P. A. Thermal Hall effect of spins in a paramagnet. *Phys. Rev. B* **91**, 125413 (2015).
- ³ Onose, Y. *et al.* Observation of the magnon Hall effect. *Science* **329**, 297-299 (2010).
- ⁴ Nasu, J., Yoshitake, J. & Motome, Y. Thermal transport in the Kitaev model. *Phys. Rev. Lett.* **119**, 127204 (2017).
- ⁵ Kasahara, Y. *et al.* Unusual thermal Hall effect in a Kitaev spin liquid candidate α -RuCl₃. *Phys. Rev. Lett.* **120**, 217205 (2018).
- ⁶ Hentrich, R. *et al.* Large thermal Hall effect in α -RuCl₃: Evidence for heat transport by Kitaev-Heisenberg paramagnons. *Phys. Rev. B* **99**, 085136 (2019).
- ⁷ Kasahara, Y. *et al.* Majorana quantization and half-integer thermal quantum Hall effect in a Kitaev spin liquid. *Nature* **559**, 227–231 (2018).
- ⁸ Hirschberger, M., Krizan, J. W., Cava, R. J. & Ong, N. P. Large thermal Hall conductivity of neutral spin excitations in a frustrated quantum magnet. *Science* **348**, 106–109 (2015).
- ⁹ Qin, T., Zhou, J. & Shi, J. Berry curvature and the phonon Hall effect. *Phys. Rev. B* **86**, 104305 (2012).
- ¹⁰ Ideue, T., Kurumaji, T., Ishiwata, S. & Tokura, Y. Giant thermal Hall effect in multiferroics. *Nature Materials* **16**, 797–802 (2017).
- ¹¹ Mori, M., Spencer-Smith, A., Sushkov, O. P. & Maekawa, S. Origin of the phonon Hall effect in rare- earth garnets. *Phys. Rev. Lett.* **113**, 265901 (2014).
- ¹² Strohm, C., Rikken, G. L. J. A. & Wyder, P. Phenomenological evidence for the phonon Hall effect. *Phys. Rev. Lett.* **95**, 155901 (2005).
- ¹³ Inyushkin, A. V. & Taldenkov, A. N. On the phonon Hall effect in a paramagnetic dielectric. *JETP Letters* **86**, 379–382 (2007)
- ¹⁴ Li, X., Fauqué, B., Zhu, Z. & Behnia, K. Phonon thermal Hall effect in strontium titanate. *Phys. Rev. Lett.* **124**, 105901 (2020).
- ¹⁵ Chen, J.-Y., Kivelson, S. A. & Sun, X.-Q. Enhanced thermal Hall effect in nearly ferroelectric insulators. *Phys. Rev. Lett.* **124**, 167601 (2020).
- ¹⁶ Grissonnanche, G. *et al.* Giant thermal Hall conductivity in the pseudogap phase of cuprate superconductors. *Nature* **571**, 376–380 (2019).
- ¹⁷ Proust, C. & Taillefer, L. The remarkable underlying ground states of cuprate

-
- superconductors. *Annual Review of Condensed Matter Physics* **10**, 409–429 (2019).
- ¹⁸ Samajdar, R. et al. Enhanced thermal Hall effect in the square-lattice Néel state. *Nature Physics* **15**, 1290–1294 (2019).
- ¹⁹ Han, J. H., Park, J.-H. & Lee, P. A. Consideration of thermal Hall effect in undoped cuprates. *Phys. Rev. B* **99**, 205157 (2019).
- ²⁰ Hess, C. et al. Magnon heat transport in doped La_2CuO_4 . *Phys. Rev. Lett.* **90**, 197002 (2003).
- ²¹ Grissonnanche, G. et al. Chiral phonons in the pseudogap phase of cuprates. *Nat. Phys.* (in press); arXiv:2003.00111 (2020).
- ²² Keimer, B. et al. Soft phonon behavior and magnetism at the low temperature structural phase transition of $\text{La}_{1.65}\text{Nd}_{0.35}\text{CuO}_4$. *Z. Physik B - Condensed Matter* **91**, 373 (1993).
- ²³ Samajdar, R., Chatterjee, S., Sachdev, S. & Scheurer, M. S. Thermal Hall effect in square-lattice spin liquids: A Schwinger boson mean-field study. *Phys. Rev. B* **99**, 165126 (2019).
- ²⁴ Slack, G. A. & Oliver, D. W. Thermal conductivity of garnets and phonon scattering by rare-earth ions. *Phys. Rev. B* **4**, 592 (1971).
- ²⁵ Li, Q. J. et al. Phonon-glass-like behavior of magnetic origin in single crystal $\text{Tb}_2\text{Ti}_2\text{O}_7$. *Phys. Rev. B* **87**, 214408 (2013).
- ²⁶ Hirokane, Y., Nii, Y., Tomioka, Y. & Onose, Y. Phononic thermal Hall effect in diluted terbium oxides. *Phys. Rev. B* **99**, 134419 (2019).
- ²⁷ Náfrádi, B. et al. Magnetostriction and magnetostructural domains in antiferromagnetic $\text{YBa}_2\text{Cu}_3\text{O}_6$. *Phys. Rev. Lett.* **116**, 047001 (2016).
- ²⁸ Ye, M., Fernandes, R. M. & Perkins, N. B. arXiv:2002.05328 (2020).
- ²⁹ Yang, Y.-F., Zhang, G.-M. & Zhang, F.-C. Universal behavior of the thermal Hall conductivity. *Phys. Rev. Lett.* **124**, 186602 (2020).
- ³⁰ Fang, Y. et al. Fermi surface transformation at the pseudogap critical point of a cuprate superconductor. arXiv:2004.01725 (2020).
- ³¹ Collignon, C. et al. Fermi-surface transformation across the pseudogap critical point of the cuprate superconductor $\text{La}_{1.6-x}\text{Nd}_{0.4}\text{Sr}_x\text{CuO}_4$. *Phys. Rev. B* **95**, 224517 (2017).
- ³² Doiron-Leyraud, N. et al. Pseudogap phase of cuprate superconductors confined by Fermi surface topology. *Nature Communications* **8**, 2044 (2017).
- ³³ Badoux, S. et al. Change of carrier density at the pseudogap critical point of a cuprate

superconductor. *Nature* **531**, 210–214 (2016).

³⁴ Ferrero, M. *et al.* Valence bond dynamical mean-field theory of doped Mott insulators with nodal/anti nodal differentiation. *EPL (Europhysics Letters)* **85**, 57009 (2009).

³⁵ Sordi, G., Haule, K. & Tremblay, A.-M. Mott physics and first-order transition between two metals in the normal-state phase diagram of the two-dimensional hubbard model. *Phys. Rev. B* **84**, 075161 (2011).

³⁶ Sordi, G., Haule, K. & Tremblay, A.-M. Finite doping signatures of the Mott transition in the two-dimensional hubbard model. *Phys. Rev. Lett.* **104**, 226402 (2010).

³⁷ Wu, W. *et al.* Pseudogap and fermi-surface topology in the two-dimensional hubbard model. *Phys. Rev. X* **8**, 021048 (2018).

³⁸ Reymbaut, A. *et al.* Pseudogap, van hove singularity, maximum in entropy, and specific heat for hole-doped Mott insulators. *Phys. Rev. Research* **1**, 023015 (2019).

³⁹ S en echal, D. & Tremblay, A.-M. Hot spots and pseudogaps for hole-and electron-doped high-temperature superconductors. *Phys. Rev. Lett.* **92**, 126401 (2004).

⁴⁰ Kyung, B., S en echal, D. & Tremblay, A.-M. Pairing dynamics in strongly correlated superconductivity. *Phys. Rev. B* **80**, 205109 (2009).

⁴¹ Scalapino, D. J. A common thread: The pairing interaction for unconventional superconductors. *Rev. Mod. Phys.* **84**, 1383 (2012).

⁴² Birgeneau, R. J. *et al.* Soft-phonon behavior and transport in single-crystal La_2CuO_4 . *Phys. Rev. Lett.* **59**, 1329-1332 (1987).

⁴³ Thio, T. *et al.* Antisymmetric exchange and its influence on the magnetic structure and conductivity of La_2CuO_4 . *Phys. Rev. B* **38**, 905–908 (1988).

⁴⁴ Sachidanandam, R., Yildirim, T., Harris, A. B., Aharony, A. & Entin-Wohlman, O. Single-ion anisotropy, crystal-field effects, spin reorientation transitions, and spin waves in R_2CuO_4 (R =Nd, Pr, and Sm). *Phys. Rev. B* **56**, 260–286 (1997).

⁴⁵ Miller, L. L. *et al.* Synthesis, structure, and properties of $\text{Sr}_2\text{CuO}_2\text{Cl}_2$. *Phys. Rev. B* **41**, 1921 (1990).

⁴⁶ Vaknin, D., Sinha, S. K., Stassis, C., Miller, L. L. & Johnston, D. C. Antiferromagnetism in $\text{Sr}_2\text{CuO}_2\text{Cl}_2$. *Phys. Rev. B* **41**, 1926 (1990).

⁴⁷ Farzaneh, M., Liu, X.-F., El-Batanouny, M. & Chou, F. C. Structure and lattice dynamics of $\text{Sr}_2\text{CuO}_2\text{Cl}_2$ (001) studied by helium-atom scattering. *Phys. Rev. B* **72**, 085409 (2005).

⁴⁸ Li, S. Y., Taillefer, L., Wang, C. H. & Chen, X. H. Ballistic magnon transport and phonon scattering in the antiferromagnet Nd_2CuO_4 . *Phys. Rev. Lett.* **95**, 156603 (2005).

⁴⁹ Li, S. Y. *et al.* Low-temperature phonon thermal conductivity of single-crystalline Nd_2CuO_4 : Effects of sample size and surface roughness. *Phys. Rev. B* **77**, 134501 (2008).